Analytica Chimica Acta 1122 (2020) 39–47

Contents lists available at ScienceDirect

Analytica Chimica Acta

journal homepage: www.elsevier.com/locate/aca

3D DNA nanonet structure coupled with target-catalyzed hairpin assembly for dual-signal synergistically amplified electrochemical sensing of circulating microRNA

Wenqing Zhang [a, 1], Huan Xu [a, 1], Xianxian Zhao [a], Xiaoqi Tang [a], Sha Yang [a], Lianyu Yu [a], Shuang Zhao [a], Kai Chang [a, **], Ming Chen [a, b, c, *]

[a] Department of Clinical Laboratory Medicine, Southwest Hospital, Third Military Medical University (Army Medical University), 30 Gaotanyan, Shapingba District, Chongqing, 400038, China
[b] College of Pharmacy and Laboratory Medicine, Third Military Medical University (Army Medical University), 30 Gaotanyan, Shapingba District, Chongqing, 400038, China
[c] State Key Laboratory of Trauma, Burn and Combined Injury, Third Military Medical University (Army Medical University), 30 Gaotanyan, Shapingba District, Chongqing, 400038, China

HIGHLIGHTS

- A 3D DNA nanonet structure was introduced for signal amplification.
- Dual amplified strategy further improved the sensitivity.
- CHA realized recognition and recycling of circulating microRNAs.
- The biosensor could achieve circulating microRNAs detection in human serum.

GRAPHICAL ABSTRACT

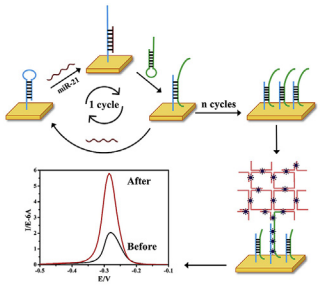

ARTICLE INFO

Article history:
Received 2 January 2020
Received in revised form
30 March 2020
Accepted 1 May 2020
Available online 5 May 2020

Keywords:
Circulating microRNA
3D DNA nanonet Structure
Catalyzed hairpin assembly
Signal amplification
Electrochemical biosensor

ABSTRACT

DNA nanomaterials are reliable and powerful tools in the development of a variety of biosensors owing to their notable self-assembly ability and precise recognition capability. Here, we propose a DNA nanomaterial-based system for the dual-amplified electrochemical sensing of circulating microRNAs by a coupled cascade of catalyzed hairpin assembly (CHA) and three-dimensional (3D) DNA nanonet structure. In the target-assisted CHA process, the stable hairpin structures H1 and H2 act as probes for the recognition and recycling of circulating microRNAs, leading to the formation of abundant H1–H2 duplexes with tails. Subsequently, a 3D DNA nanonet structure was introduced, which was assembled using three DNA strands constructed X-DNA monomers as the building blocks, and hybridized to the tails of H1–H2 duplexes. The successful integration of target-assisted CHA and 3D DNA nanonet structure induced the second signal amplification. The designed biosensor performed under optimized experimental conditions, and exposed admirable analytical performance for the detection of circulating miR-21, with a wide linear range from 10 fM to 1 nM, high sensitivity of limit of detection (LOD) of 3.6083 fM, good

* Corresponding author. Department of Clinical Laboratory Medicine, Southwest Hospital, Third Military Medical University (Army Medical University), 30 Gaotanyan, Shapingba District, Chongqing, 400038, China.
** Corresponding author.
E-mail addresses: changkai0203@163.com (K. Chang), chming1971@126.com (M. Chen).
[1] Contributed equally.

https://doi.org/10.1016/j.aca.2020.05.002

specificity in the face of single nucleotides and other microRNAs, satisfactory stability and reproducibility for practical analysis. Furthermore, the clinical applicability for circulating miR-21 detection was verified in human serum samples without additional treatment. We hope that this elaborated biosensor will provide new opportunities for bioassays based on DNA nanomaterials.

1. Introduction

Circulating microRNAs (miRNAs) are classified as small non-coding RNAs secreted from living cells into the extracellular environment [1,2]. They remain remarkably stable [3] in various bodily fluids such as the blood, urine, bile, cerebrospinal fluid, and pancreatic juice [4]. Owing to their advantages such as tissue-specific origin, rich information content, and availability [5], circulating miRNAs have been proven to serve as ideal non-invasive biomarkers for the clinical diagnosis of numerous diseases, such as cancer [6–8], bone loss disorders [9], psychiatric disorders [10], cardiovascular disease [11], and radiation exposure [12]. However, the clinical application of circulating miRNA-based detection has been limited due to their relatively low abundance in the extracellular environment, small size, and sequence homology with other miRNAs [13]. At present, a variety of emerging biosensing techniques, such as fluorescence detection [14,15], micro-fluidic devices [16], electrochemiluminescence (ECL) [17,18], colorimetric assays [19,20] and electrochemistry [21,22] have been applied for miRNAs detection. Among these methods, use of an electrochemical biosensor is considered particularly a promising strategy for detecting circulating miRNAs, owing to its high sensitivity, less sample requirements, easy controllability, and low cost [23].

DNA as a natural biomaterial exhibits a series of outstanding properties compared with synthetic materials, including great self-assembly ability, perfect programmability, and precise recognition capability [24]. So, DNA-based nanomaterials, such as DNA walker [25,26], DNA nanotweezer [27], DNA tetrahedron [28,29], and DNA hydrogels [30], provide wide applications for the development of biosensors [31]. Among the possible DNA nanostructures, X-shaped DNA (X-DNA) [32,33] is composed of four oligonucleotides, with each arm possessing a complementary sticky end and phosphate groups that can be ligated with each other. X-DNA-based DNA hydrogels have a centimeter scale size, exhibited characteristics of stability, high selectivity, and high operability. They have been used for diverse applications [34], including visualized detection of glucose [35], cell-free protein synthesis system [36], and unique energy storage device [37]. Inspired by this X-DNA cross-linked DNA hydrogel, we developed a three-dimensional (3D) DNA nanonet structure based on the directional assembly of improved X-DNA monomers, which was constituted by only three DNA strands, unlike the conventional four DNA strands. The 3D DNA nanonet structure was obtained by the self-assembly of X-DNA coupled with T4 DNA ligase-catalyzed reactions. Compared with X-DNA, the monomers stacking 3D DNA nanonet structure showed an extremely larger scale, suggesting its application potential in biosensor field to meet signal amplification requirements.

Numerous signal-amplified technologies have been developed for miRNAs detection to date, including rolling circle amplification (RCA) [38,39], hybridization chain reaction (HCR) [40], strand displacement amplification (SDA) [41], and catalyzed hairpin assembly (CHA) [42]. Among these, target-assisted CHA is widely accepted approach to amplify the signal of various biomarkers *in vitro* and in living cells, including DNA, mRNA, proteins, and cancer cells, due to its high amplification efficiency, enzyme-free and isothermal amplification, and easy operation [43]. In brief, CHA consists of two substrate hairpin sequences, which hybridize autonomously once triggered by the target, resulting in thermodynamically stable duplexes. While considering the low abundance of circulating miRNAs in extracellular environment, circulating miRNAs detection requires more efficient signal amplification. Currently, cascade of multiple amplification strategies attracts considerable attention, which can exhibit promising performance of diverse biosensors [44,45]. Thus, owing to versatility and exponential amplification efficiency of CHA reaction, it can be integrated with other DNA nanostructures, achieving cascade signal amplification.

Based on the above context, we proposed a DNA nanomaterial-based dual signal synergistically amplified electrochemical biosensor using cascade of CHA and 3D DNA nanonet structure for circulating miR-21 detection, as the abnormal expression of miR-21 has been associated with several types of cancer [46–48]. Thus, we designed an improved CHA process for specific target selection and cascade target cycling, which effectively overcame the difficulties in the detection of the small and unstable, but clinically relevant, miR-21. The conversion and amplification of miR-21 were achieved by sustained cyclic reaction between hairpin probes of H1 and H2. As a result, abundant H1–H2 duplexes with tails were obtained. The tails of H1–H2 duplexes could form the fourth arm of the improved X-DNA by complementary base pairs, thus enabling specific hybridization to the 3D DNA nanonet structure to achieve the second signal amplification. The extremely large scale of 3D DNA nanonet structure remarkably amplified signal again by providing a landing for the subsequent electroactive molecule of methylene blue. This synergetic amplification strategy achieved ultrasensitive and specificity detection of the circulating miRNA, which offer a new perspective for the broader application of DNA nanomaterials in biosensing.

2. Experimental

2.1. Reagents

The sequences of DNA and RNA were manufactured and purified by high-performance liquid chromatography (HPLC) from TaKaRa Biotechnology Company (Dalian, China). The detailed sequences of DNAs/RNAs used in experiments are shown in Table S1. Potassium ferrocyanide ($K_4Fe(CN)_6$), Potassium hexacyanoferrate (III) ($K_3Fe(CN)_6$), tris (2-carboxyethyl) phosphine hydrochloride (TCEP), blue dextran, methylene blue (MB), and 6-mercapto-1-hexanol (MCH) were purchased from Sigma-Aldrich (St Louis, MO, USA). The Super GelRed nuclear staining was purchased from US Everbright Inc (China). Blue/Orange 6 × Loading Dye was obtained from Promega Corporation (Madison, WI, USA). The 20 bp DNA Ladder was purchased from TaKaRa Biotechnology Company (Dalian, China). T4 DNA ligase (M0202L) was purchased from New England Biolabs Inc (Beverly, MA, USA). 5 × TBE buffer, 30% Acr-Bis (29:1), and Phosphate-buffered saline (PBS) buffer (0.01 M, pH 7.2–7.4) were obtained from Solarbio Life Sciences (Beijing, China). Immobilization buffer (12.5 mM magnesium acetate, 40 mM Trisbase,

2 mM EDTA, 20 mM acetic acid, pH 7.4) and hybridization buffer (50 mM PBS, 0.5 M NaCl, pH 7.4) were prepared in our laboratory. The ultrapure water used in this work was 18.2 MΩcm (Millipore, USA). All chemical reagents belong to the analytical reagent grade. The human serum samples were collected and ethical approval was obtained from Southwest Hospital (China) of Third Military Medical University.

2.2. Apparatus and experimental parameters

A CHI 760E electrochemical workstation (Shanghai Chenhua, China) was used to operate electrochemical procedures. A conventional three-electrode system was employed in this study, where a modified gold electrode as the working electrode, platinum electrode as the counter electrode, and saturated calomel electrode as the reference electrode. Electrochemical measurements included cyclic voltammetry (CV), electrochemical impedance spectroscopy (EIS), and differential pulse voltammetry (DPV). CV and EIS were processed in 10 mM $[Fe(CN)6]^{3-/4-}$ (0.1 M KCl, 0.01 M PBS) to verify the feasibility of biosensor. Particularly, CV was carried out of range from −0.2 V to 0.6 V under a scan rate of 100 mV/s. EIS was measured with frequency range of 0.1–10^5 Hz and an amplitude of 5 mV. DPV was carried out in the working solution (50 mM NaCl, 10 mM Tris-HCL) with a potential range of −0.1 V to −0.6 V, pulse amplitude of 0.01 V, pulse width of 0.05 s, and sampling width of 0.0167 s. Bio-Rad imaging system (California, USA) was used to operate native polyacrylamide gel electrophoresis (PAGE). The pH of buffer solutions was measured with the FE28 pH-meter of METTLER TOLEDO (Shanghai, China).

2.3. Construction and confirmation of 3D DNA nanonet structure

The 3D DNA nanonet structure was prepared by ligating a large number of X-DNA monomers, comprising three single-stranded DNA (ssDNA). Each arm of X-DNA monomer possessed a complementary sticky end and phosphate groups that can be ligated to each other via T4 DNA ligase. A typical 20-μL reaction system containing 2 μL each of X1-P, X2-P, and X3-P (10 μM), 2 μL 10 × T4 DNA ligase reaction buffer, and 11.5 μL DNase/RNase-Free water, which were mixed well gently. The mixture was first heated at 95 °C for 2 min, then dropped to 65 °C for 5 min, cooled to 60 °C for 3 min, and finally slowly annealed to 25 °C for 1 h to form X-DNA. Subsequently, 0.5 μL T4 DNA ligase was mixed and kept the reaction system at 16 °C for 10 min to form the 3D DNA nanonet structure. The final products were diluted to 0.5 μM by hybridization buffer and stored at 4 °C.

12% PAGE and blue dextran solution were used to confirm and analyze the 3D DNA nanonet structure. In brief, 5 μL reaction products with 1 μL 6 × Loading Dye were loaded onto relevant lane and a voltage of 120 V was applied for 55 min. The bands were dyed with Super GelRed nuclear staining, then imaged using Bio-Rad Imaging System. Furthermore, 2 μM blue dextran solution with 150 mM NaCl was layered onto the DNA samples and allowed to settle naturally, followed by visual interpretation.

2.4. Fabrication of dual amplified electrochemical biosensor

The gold electrode was cleaned using routine methods. First, gold electrode was polished with aluminum slurry (0.3 μm and 0.05 μm, respectively) carefully, followed by 1 min sonication in absolute ethanol and ultrapure water sequentially to get rid of surface deposits. Subsequently, the polished electrode was immersed in a fresh piranha solution (30% hydrogen peroxide: 98% sulfuric acid = 1: 3) for 10 min to clean further. After each step, the electrode was cleaned with ultrapure water and desiccated with high-purity nitrogen well.

H1 and H2 probes were first pretreated by heating at 95 °C for 10 min, then gradually dropped to 25 °C. Afterwards, 2 μM H1 (diluted by immobilization buffer) mixed with 1 mM TCEP, which could reduce the formation of disulfide bonds to enhance the density of H1, and then dropped onto the prepared gold electrode at 37 °C overnight to obtain Au/H1. The electrode was then blocked by 1 mM MCH at 4 °C for 1 h. Subsequently, 4 μL hybridization buffer containing different concentrations of synthesized miR-21 and 2 μM H2 were dropped onto the electrode at 37 °C for 90 min for the CHA process. To implement second signal amplification, 4 μL solution of 3D DNA nanonet structure was introduced to the system, followed by incubation at 37 °C for 90 min. Notably, the gold electrode was carefully rinsed with 0.01 M PBS and dried with nitrogen after each modification. The final modified electrode was treated with 1 mM MB solution (10 mM Tris-HCL, 50 mM NaCl) and stored at 25 °C for 30 min in dark. After rinsing with ultrapure water, the electrochemical signal of MB was measured by DPV.

3. Results and discussion

3.1. Experimental principle of dual amplified biosensing strategy

A schematic illustration of this proposed DNA nanomaterial based dual-amplified electrochemical sensing system for circulating miRNA detection is shown in Scheme 1. The strategy consists of two signal amplification processes: the target-assisted CHA process and self-assembly 3D DNA nanonet structure. First, the H1 was modified on the bare gold electrode via combination of Au–S binding. Subsequently, miR-21 and H2 were introduced to induce the CHA reaction. Minimal spontaneous interaction between H1 and H2 probes without initiated by miR-21 for the stability of hairpin structure. Once triggered by the miR-21, H1 and H2 could continuously hybridize autonomously, resulting in thermodynamically stable H1–H2 duplexes. Meanwhile, miR-21 was released for the next cycle to achieve the first signal amplification. The 3D DNA nanonet structure was ligated with a large amount of three-armed X-DNA monomer, in which each arm possesses a complementary sticky end and phosphate groups that can be ligated coupled with T4 DNA ligase-catalyzed reactions. The use of three-armed X-DNA is critical for the second signal amplification, as the tails of the H1–H2 duplexes produced from the CHA process form the fourth arm of the X-DNA, thus enabling specific hybridization to the 3D DNA nanonet structure to achieve the second signal amplification. Moreover, MB molecules were used as electrochemical probe, which can specifically intercalate these huge DNA duplexes. Therefore, the electrochemical signal of methylene blue is in linear correlation with the concentration of circulating miR-21. Until now, dual amplified electrochemical biosensors for circulating miRNA detection had been achieved.

3.2. Formation of the 3D DNA nanonet structure

PAGE analysis of the X-DNA and 3D DNA nanonet structure demonstrated the formation of a larger DNA structure as the number of ssDNAs increased, as evidenced by slower mobility of the band on the gel (Fig. 1A). Specifically, the band corresponding to the 3D DNA nanonet structure did not move owing to its very high molecular weight, indicating that the 3D DNA nanonet structure was fabricated successfully. The blue dextran solution with 2 × 10^6 molecular weight was also used to demonstrate formation of the 3D DNA nanonet structure (Fig. 1B). X-DNA was above the blue dextran solution owing to its smaller molecular weight and smaller density, whereas the 3D DNA nanonet structure was deposited below the tube because of its larger molecular weight. Collectively,

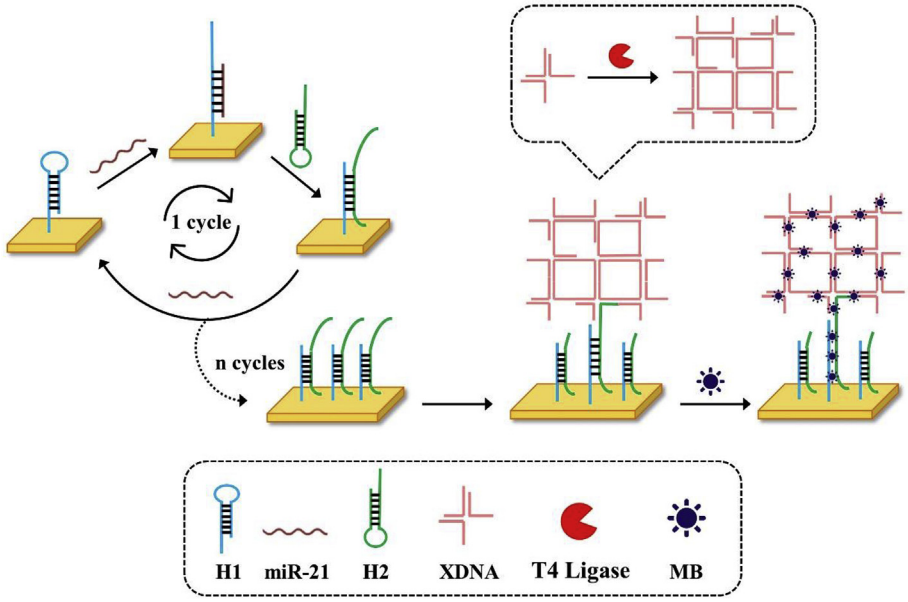

Scheme 1. Schematic illustration of dual amplified electrochemical sensing of circulating microRNA based on cascade of catalyzed hairpin assembly (CHA) and DNA nanonet structure.

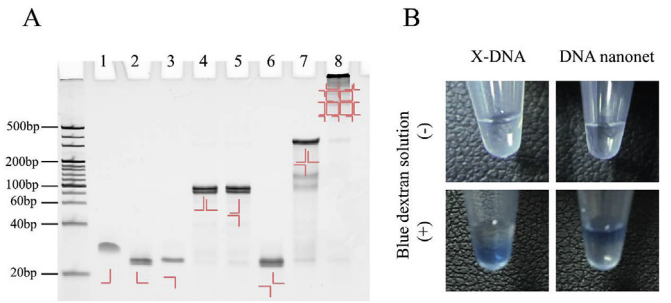

Fig. 1. PAGE analysis of formation of the X-DNA and DNA nanonet structure (A). Each lane contains 1 μM DNA products. X1-P (Line 1), X2-P (Line 2), X3-P (Line 3), X1-P/X2-P (Line 4), X1-P/X3-P (Line 5), X2-P/X3-P (Line 6), X1-P/X2-P/X3-P (Line 7), DNA nanonet structure (Line 8); Images of X-DNA and DNA nanonet structure before (−) and after (+) the addition of blue dextran solution (B).

these results demonstrated that the X-DNA and 3D DNA nanonet structure were constructed successfully.

3.3. Feasibility of the dual amplified biosensing strategy

PAGE, DPV, CV and EIS analysis verified the feasibility of the biosensing strategy (Fig. 2). Fig. 2A displayed the result of PAGE analysis. Specifically, Lane1, 2, and 3 corresponded to H1, H2, and miR-21 probe respectively. There was a weak band of hybridization between H1 and H2 without miR-21 (Lane 4), whereas a significant band of hybridization was observed under the assistance of miR-21 (Lane 5). Lane 6–8 showed the assembly process of the 3D DNA nanonet structure, similar to Fig. 1A. The band at the highest position (Lane 9) represented the result of hybridization of the products of CHA with the 3D DNA nanonet structure, and the band at the lowest position corresponded to the miR-21 released in the process of CHA, confirming the successful assembly process and the interactions among these DNA sequences.

The DPV signal of MB with a significant peak current at around −0.285 V was used to verify the fabrication process of the biosensor (Fig. 2B). First, the electrode modified with H1 and MCH showed a lower peak (black line). After incubating with H2 and miR-21, an obvious increase was observed owing to the first signal amplification by CHA (red line). Finally, a marked increase in the DPV signal was observed owing to the combination of CHA and 3D DNA nanonet structure (blue line).

CV (Fig. 2C) and EIS (Fig. 2D) were also carried out to characterize the stepwise fabrication of the biosensor. The bare gold electrode had well-defined CV redox peaks and showed small electron transfer resistance (R_{et}) of 152 Ω (curve a). Afterwards, when gold electrode was modified by H1, CV redox peaks were reduced and the R_{et} increased to 386 Ω (curve b) due to the more negative charges of H1 that would reduce the electrons transmission of $[Fe(CN)6]^{3-/4-}$. Subsequently, CV redox peaks and R_{et} continued to reduce and increase after the addition of MCH (curve c), H2 and miR-21 (curve d), which was ascribed to a further increase in the R_{et} (from 3187 Ω to 3820 Ω). Finally, after introduction of the 3D DNA nanonet structure to the surface of the electrode, CV redox peaks were further decreased and R_{et} dramatic increased to 7908 Ω (curve e) due to more negative charges of this huge construction. These results verified that the electrochemical biosensor was successfully assembled.

3.4. Optimization of the dual amplified biosensing strategy

Six experimental parameters including the concentration of H2 and H1, reaction time and temperature of CHA, and concentration and incubation time of 3D DNA nanonet structure, were investigated to maximize the sensitivity and efficiency of our method. When the concentration of H2 or H1 was increased from 0.5 to 2.5 μM, the DPV response increased, reaching the maximum at 2 μM, followed by a gradual decrease (Fig. 3A and B). Hence, the optimum concentration of both H1 and H2 was 2 μM. Furthermore, the DPV response increased with the reaction time of CHA range from 0.5 to 2.5 h, reaching a plateau at 1.5 h, which indicated that the best result could be obtained at this time (Fig. 3C). The reaction temperature of CHA was also found to be a critical factor for the efficiency of the reaction. When the electrode was incubated at 27 °C, 32 °C, 37 °C, 42 °C and 47 °C, the DPV response initially increased, attained the maximal value at 37 °C, and then decreased

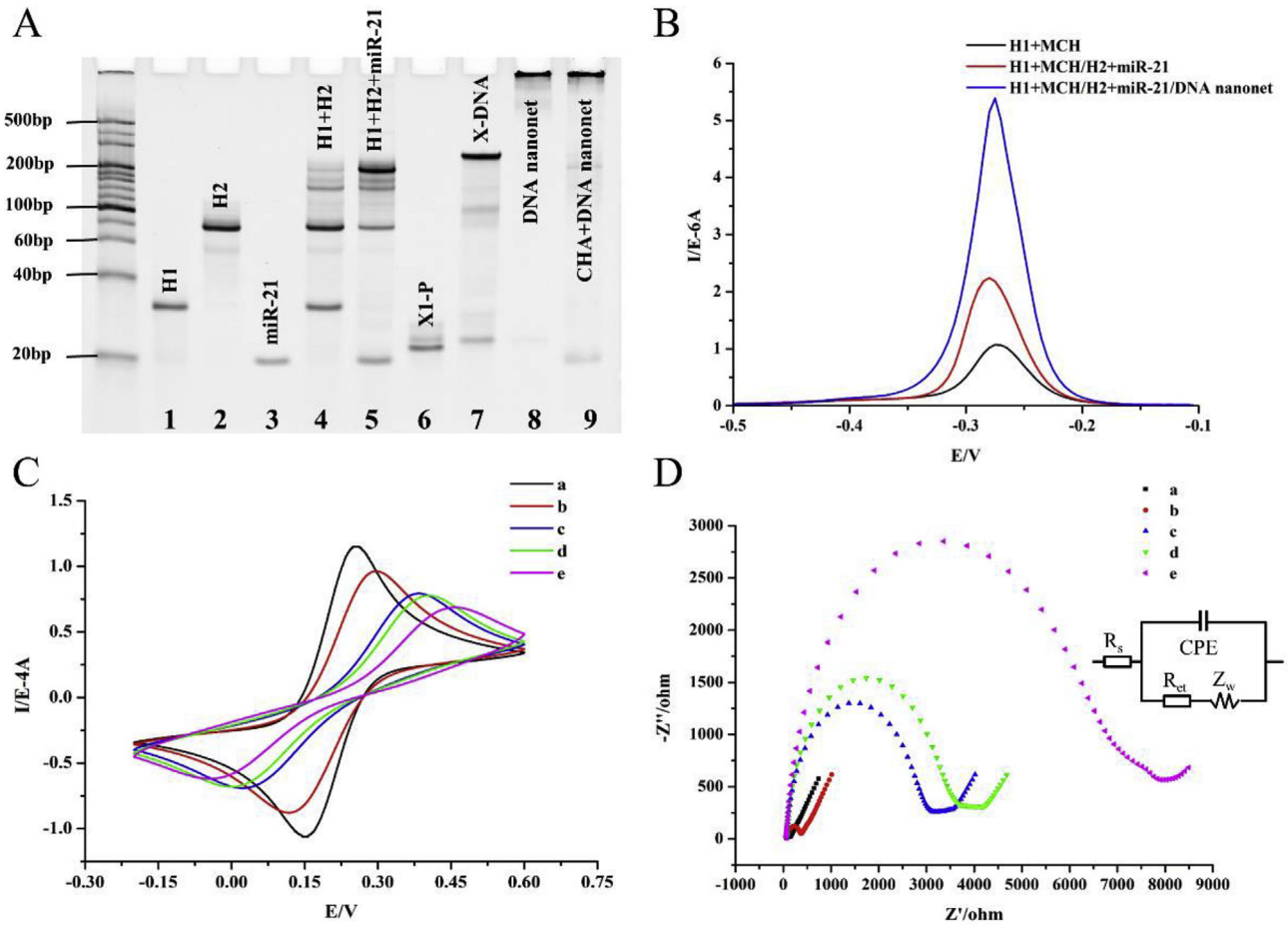

Fig. 2. PAGE (A) characteristics of CHA-DNA nanonet structure products, each lane contains 1 μM DNA products; DPV (B) characteristics of CHA-DNA nanonet structure products; CV (C) and EIS (D) characteristics of different modified electrode, bare Au electrode (Au) (a), H1/Au (b), MCH/H1/Au (c), H2 + miR-21/MCH/H1/Au (d), DNA nanonet/H2 + miR-21/MCH/H1/Au (e). Insert figure of D was equivalent circuit to simulate the EIS data.

up to 47 °C (Fig. 3D). Consequently, an optimum reaction temperature of CHA was 37 °C. Moreover, DPV response enhanced as the concentration of 3D DNA nanonet structure range from 0.1 to 0.5 μM and then slowly decreased up to 1 μM, indicating an optimum probe concentration of 0.5 μM (Fig. 3E). The DPV response increased with increasing incubation time of the 3D DNA nanonet structure range from 0.5 to 2.5 h, and reached a plateau at 1.5 h, which was determined as the optimal incubation time (Fig. 3F).

3.5. Performance of the dual amplified biosensing strategy

To assess the detection performance, the biosensing system was applied for the quantitative detection of miR-21 according to DPV, as the DPV peak current was attributed to the oxidation of MB on the DNA duplex. The DPV peak current elevated with the increment of miR-21 concentration from 0 to 10 nM (Fig. 4A). Furthermore, the relationship between DPV response value and the logarithm of miR-21 concentrations (10 fM to 1 nM) could be described as a linear regression equation of $I = 0.6508 \lg c + 1.900$, with $R^2 = 0.9980$ (where I represents the DPV peak current and c represents the concentration of miR-21) (Fig. 4B). Besides, the limit of detection (LOD) was determined to be 3.6083 fM, as the LOD = $3 S_b/k$ (where S_b represents the standard deviation of the blank, k represents the slope of the corresponding calibration curve, n = 5). Compared with previously reported miRNA biosensors (Table S2), our dual amplified biosensor has a lower LOD and a relatively wider linear range, providing more effective method for quantifying circulating miR-21.

3.6. Specificity, stability and reproducibility of the dual amplified biosensing strategy

To further investigate the specificity of our method, miR-21 and seven different kinds of control samples were detected under the same experiment condition, including blank, single-base mismatched miR-21 (Miss-1), double-base mismatched miR-21 (Miss-2), three-base mismatched miR-21 (Miss-3), miR-107, miR-145 and miR-25. Fig. 5 shows that significant enhancement of the DPV response was obtained with target miR-21, whereas only a small current response was obtained with the control samples, demonstrating that the sensor had superior ability to distinguish base mutations and other interference miRNA sequences. Moreover, the stability of the biosensor was appraised by quantitative detection of miR-21 every 5 days with the H1 probe-modified electrodes. After 15 days, the biosensor maintained 75.45% of the corresponding initial response, which is satisfactory for practical application (Fig. S1). Meanwhile, the reproducibility of the proposed biosensor was evaluated by analyzing miR-21 (1 nM) with 10 individual electrodes under the same condition. The relative standard deviation (RSD) was 7.99%, indicating the satisfactory reproducibility of the proposed biosensor for detecting circulating miR-21 (Table S3).

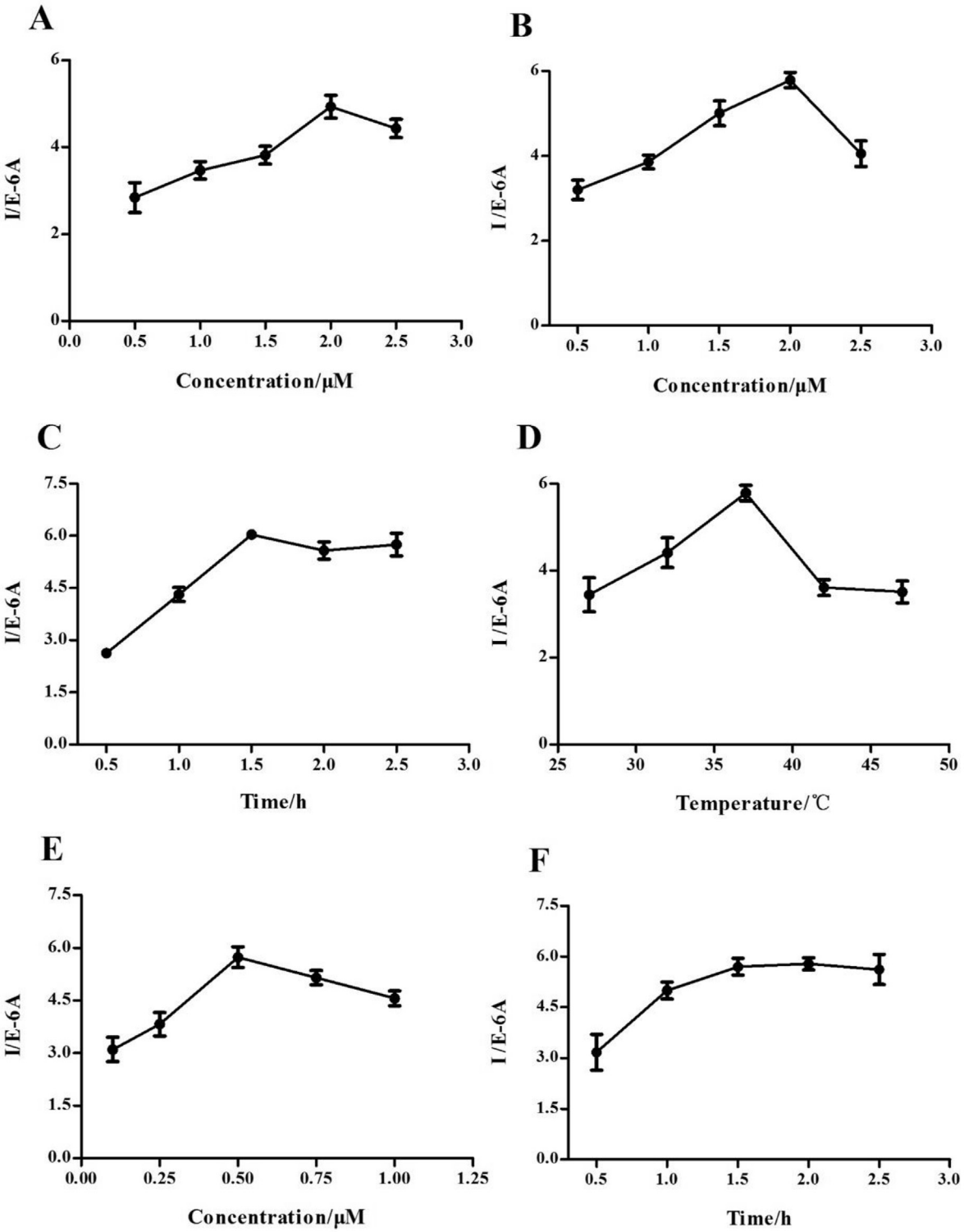

Fig. 3. Optimizations of experimental parameters: concentration of H2 probes (A), concentration of H1 probes (B), reaction time of CHA (C), reaction temperature of CHA (D), concentration of DNA nanonet structure (E), reaction time of DNA nanonet structure hybridization (F). The concentration of miR-21 was 1 nM, and the error bars represent the standard deviations of five measurements.

3.7. Application of the dual amplified biosensing strategy in human serum

Finally, to evaluate the clinical application of the fabricated biosensor, various concentrations of miR-21 (100 fM, 1 pM, 10 pM, 100 pM) were detected in healthy human serum samples 10-fold diluted by hybridization buffer. The DPV signal of the spiked samples was analyzed with the linear regression equation given above to calculate the measured concentration. Table 1 presents that the RSD ranged from 1.28% to 11.17% and the recovery ranged from

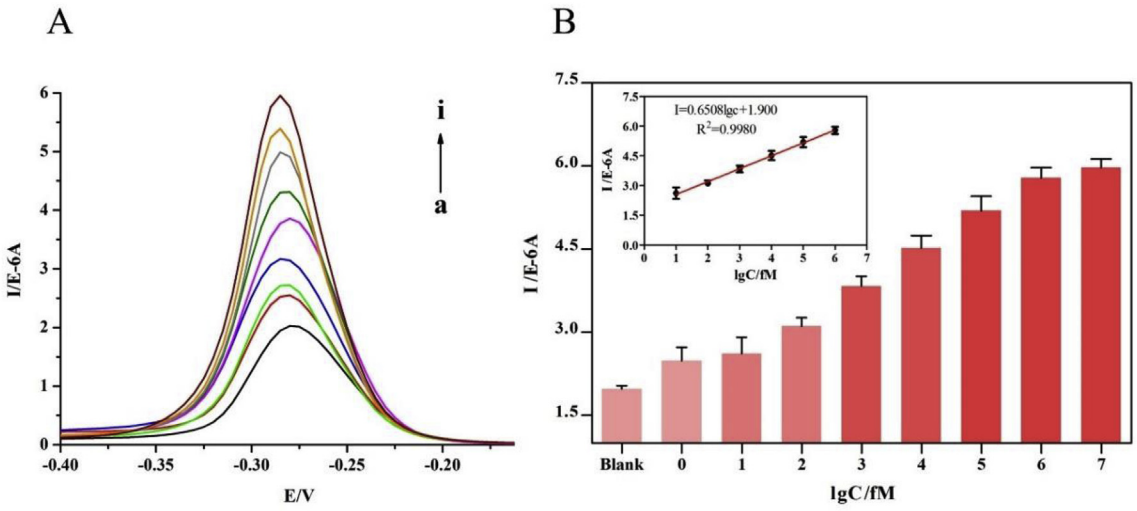

Fig. 4. DPV current responses (A) of dual amplified electrochemical biosensor to different concentration of the target miRNA. From a to i: 0, 1 fM, 10 fM, 100 fM, 1 pM, 10 pM, 100 pM, 1 nM and 10 nM; Calibration plot between the DPV peak current and the logarithm of target miRNA concentrations in the range from 10 fM to 1 nM (B). The error bars represent the standard deviations of five measurements.

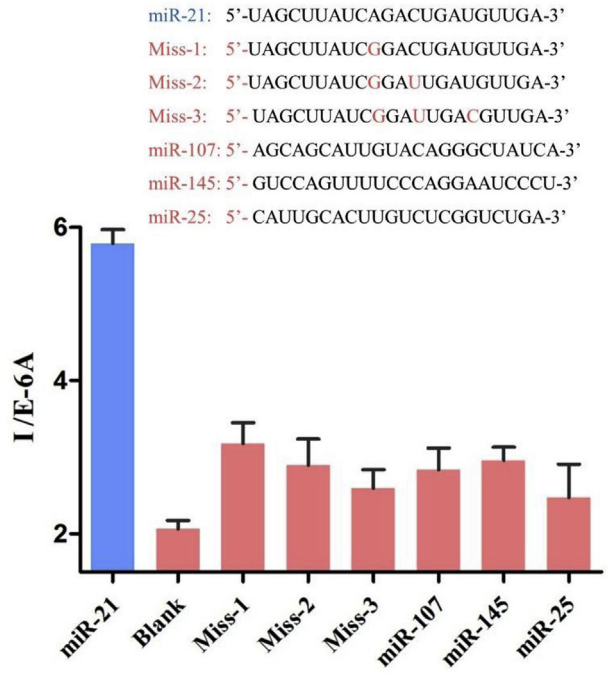

Fig. 5. Specificity of the proposed electrochemical biosensor. Comparing the DPV peak current of target miR-21 with seven control samples including blank, the single-base mismatched miR-21 (Miss-1), double-bases mismatched miR-21 (Miss-2), three-bases mismatched miR-21 (Miss-3), miR-107, miR-145 and miR-25. The concentration of all samples was 1 nM, and the error bars represent the standard deviations of five measurements.

Table 1
Determination results of different concentration of target miRNA in human serum samples by using proposed electrochemical biosensor (n = 3).

Added	Measured	Recovery (%)	RSD (%)
100 fM	97.72 fM	97.72	9.36
1 pM	0.93 pM	93.30	11.17
10 pM	11.07 pM	110.70	1.28
100 pM	108.22 pM	108.22	4.64

93.30% to 110.70%. This result proved that the dual amplified CHA-3D DNA nanonet structure electrochemical biosensor could directly detect circulating miRNA in complex biological samples, which could facilitate the clinical application.

4. Conclusions

In summary, we have proposed a DNA nanomaterial based dual-signal amplification electrochemical biosensor and successfully applied it for ultrasensitive detection of circulating miR-21. Dual-signal amplification was obtained through the integration of target-triggered CHA and 3D DNA nanonet structure based on the improved X-DNA monomers. The proposed biosensor demonstrated a linear relationship with the concentration of miR-21 ranging from 10 fM to 1 nM, and a detection limit of 3.6083 fM was achieved. In addition, we also verified clinical application of the proposed biosensor for detection of circulating miR-21 in human serum. Therefore, the DNA nanomaterial based dual-signal amplification electrochemical biosensor may provide more effective and accurate diagnosis and prognosis evaluation for miRNA-associated diseases. Future investigation will be focused on improving the capabilities of simultaneous detection of more circulating miRNAs. We expected that the proposed biosensor would provide a brand-new opportunity for bioassays based on DNA nanomaterials in living systems and extend to point-of-care applications. However, more detailed future work is required before the clinical application.

Author contributions

The manuscript was written through contributions of all authors. Authors have given approval to the final version of the manuscript.

Declaration of competing interest

The authors declare that they have no known competing financial interests or personal relationships that could have appeared to influence the work reported in this paper.

CRediT authorship contribution statement

Wenqing Zhang: Conceptualization, Formal analysis, Investigation, Writing - original draft. **Huan Xu:** Conceptualization, Methodology, Writing - review & editing. **Xianxian Zhao:** Investigation, Formal analysis, Writing - review & editing. **Xiaoqi Tang:** Software, Investigation, Formal analysis. **Sha Yang:** Validation, Resources, Formal analysis. **Lianyu Yu:** Validation, Software. **Shuang Zhao:** Validation, Visualization. **Kai Chang:** Methodology, Writing - review & editing, Supervision. **Ming Chen:** Conceptualization, Writing - review & editing, Supervision, Funding acquisition.

Acknowledgements

This work was supported by the National Natural Science Foundation of China (Grant No. 81430053, 81972027), the Innovation Project of the First Affiliated Hospital of Army Medical University (SWH2019QNKJ-04), the Clinical Technology Innovation Project of the Army Medical University (CX2019JS105).

Appendix A. Supplementary data

Supplementary data to this article can be found online at https://doi.org/10.1016/j.aca.2020.05.002.

References

[1] C. Ji, X. Guo, The clinical potential of circulating microRNAs in obesity, Nat. Rev. Endocrinol. 15 (2019) 731–743.
[2] S. Salloum-Asfar, N.J. Satheesh, S.A. Abdulla, Circulating miRNAs, small but promising biomarkers for autism spectrum disorder, Front. Mol. Neurosci. 12 (2019) 253.
[3] F. Balzano, M. Deiana, S. Dei Giudici, A. Oggiano, A. Baralla, S. Pasella, A. Mannu, M. Pescatori, B. Porcu, G. Fanciulli, A. Zinellu, C. Carru, L. Deiana, miRNA stability in frozen plasma samples, Molecules 20 (2015) 19030–19040.
[4] A. Mohr, J. Mott, Overview of MicroRNA biology, Semin. Liver Dis. 35 (2015) 3–11.
[5] C.C. Pritchard, H.H. Cheng, M. Tewari, MicroRNA profiling: approaches and considerations, Nat. Rev. Genet. 13 (2012) 358–369.
[6] P.S. Mitchell, R.K. Parkin, E.M. Kroh, B.R. Fritz, S.K. Wyman, E.L. Pogosova-Agadjanyan, A. Peterson, J. Noteboom, K.C. O'Briant, A. Allen, D.W. Lin, N. Urban, C.W. Drescher, B.S. Knudsen, D.L. Stirewalt, R. Gentleman, R.L. Vessella, P.S. Nelson, D.B. Martin, M. Tewari, Circulating microRNAs as stable blood-based markers for cancer detection, Proc. Natl. Acad. Sci. U.S.A. 105 (2008) 10513–10518.
[7] M. Pichler, G.A. Calin, MicroRNAs in cancer: from developmental genes in worms to their clinical application in patients, Br. J. Canc. 113 (2015) 569–573.
[8] M.J. Murray, R.A. Huddart, N. Coleman, The present and future of serum diagnostic tests for testicular germ cell tumours, Nat. Rev. Urol. 13 (2016) 715–725.
[9] M. Sun, L. Hu, S. Wang, T. Huang, M. Zhang, M. Yang, W. Zhen, D. Yang, W. Lu, M. Guan, S. Peng, Circulating MicroRNA-19b identified from osteoporotic vertebral compression fracture patients increases bone formation, J. Bone Miner. Res. 35 (2019) 306–316.
[10] O. Issler, A. Chen, Determining the role of microRNAs in psychiatric disorders, Nat. Rev. Neurosci. 16 (2015) 201–212.
[11] X. Luo, B. Yang, S. Nattel, MicroRNAs and atrial fibrillation: mechanisms and translational potential, Nat. Rev. Cardiol. 12 (2015) 80–90.
[12] B. Małachowska, B. Tomasik, K. Stawiski, S. Kulkarni, C. Guha, D. Chowdhury, W. Fendler, Circulating microRNAs as biomarkers of radiation exposure: a systematic review and meta-analysis, Int. J. Radiat. Oncol. Biol. Phys. 106 (2019) 390–402.
[13] A.R. Chandrasekaran, J.A. Punnoose, L. Zhou, P. Dey, B.K. Dey, K. Halvorsen, DNA nanotechnology approaches for microRNA detection and diagnosis, Nucleic Acids Res. 47 (2019) 10489–10505.
[14] K. Quan, J. Li, J. Wang, N. Xie, Q. Wei, J. Tang, X. Yang, K. Wang, J. Huang, Dual-microRNA-controlled double-amplified cascaded logic DNA circuits for accurate discrimination of cell subtypes, Chem. Sci. 10 (2019) 1442–1449.
[15] Z. Liu, Y. Wang, J. Li, Y. Yuan, X. Wu, W. Liu, Y. Liu, A label-free fluorescent enhancement nanosensor for ultrasensitive and highly selective detection of miRNA-378 through signal synergy amplification, Anal. Chim. Acta 1087 (2019) 86–92.
[16] R. Bruch, J. Baaske, C. Chatelle, M. Meirich, S. Madlener, W. Weber, C. Dincer, G.A. Urban, CRISPR/Cas13a-Powered electrochemical microfluidic biosensor for nucleic acid amplification-free miRNA diagnostics, Adv. Mater. 31 (2019), e1905311.
[17] Y. Zhang, Y. Chai, H. Wang, R. Yuan, Target-induced 3D DNA network structure as a novel signal amplifier for ultrasensitive electrochemiluminescence detection of MicroRNAs, Anal. Chem. 91 (2019) 14368–14374.
[18] L. Lu, C. Liu, W. Miao, X. Wang, G. Guo, Ultrasensitive detection of miRNA based on efficient immobilization of probe and electrochemiluminescent quenching of Ru(bpy)32+ by methylene blue, Anal. Chim. Acta 1093 (2020) 52–60.
[19] D. Li, W. Cheng, Y. Yan, Y. Zhang, Y. Yin, H. Ju, S. Ding, A colorimetric biosensor for detection of attomolar microRNA with a functional nucleic acid-based amplification machine, Talanta 146 (2016) 470–476.
[20] Y. Zhang, I.D. McKelvie, R.W. Cattrall, S.D. Kolev, Colorimetric detection based on localised surface plasmon resonance of gold nanoparticles: merits, inherent shortcomings and future prospects, Talanta 152 (2016) 410–422.
[21] X. Zhang, Z. Yang, Y. Chang, M. Qing, R. Yuan, Y. Chai, Novel 2D-DNA-nanoprobe-mediated enzyme-free-target-recycling amplification for the ultrasensitive electrochemical detection of MicroRNA, Anal. Chem. 90 (2018) 9538–9544.
[22] X. Chen, L. Yao, Y. Wang, Q. Chen, H. Deng, Z. Lin, H. Yang, Novel electrochemical nanoswitch biosensor based on self-assembled pH-sensitive continuous circular DNA, Biosens. Bioelectron. 131 (2019) 274–279.
[23] M. Labib, M.V. Berezovski, Electrochemical sensing of microRNAs: avenues and paradigms, Biosens. Bioelectron. 68 (2015) 83–94.
[24] S. Nummelin, J. Kommeri, M.A. Kostiainen, V. Linko, Evolution of structural DNA nanotechnology, Adv. Mater. 30 (2018), e1703721.
[25] X. Yang, Y. Tang, S.D. Mason, J. Chen, F. Li, Enzyme-powered three-dimensional DNA nanomachine for DNA walking, payload release, and biosensing, ACS Nano 10 (2016) 2324–2330.
[26] Z. Xu, L. Liao, Y. Chai, H. Wang, R. Yuan, Ultrasensitive electrochemiluminescence biosensor for MicroRNA detection by 3D DNA walking machine based target conversion and distance-controllable signal quenching and enhancing, Anal. Chem. 89 (2017) 8282–8287.
[27] D. Li, W. Cheng, Y. Li, Y. Xu, X. Li, Y. Yin, H. Ju, S. Ding, Catalytic hairpin assembly actuated DNA nanotweezer for logic gate building and sensitive enzyme-free biosensing of MicroRNAs, Anal. Chem. 88 (2016) 7500–7506.
[28] M. Lin, P. Song, G. Zhou, X. Zuo, A. Aldalbahi, X. Lou, J. Shi, C. Fan, Electrochemical detection of nucleic acids, proteins, small molecules and cells using a DNA-nanostructure-based universal biosensing platform, Nat. Protoc. 11 (2016) 1244–1263.
[29] F. Xu, H. Dong, Y. Cao, H. Lu, X. Meng, W. Dai, X. Zhang, K.A. Al-Ghanim, S. Mahboob, Ultrasensitive and multiple disease-related MicroRNA detection based on tetrahedral DNA nanostructures and duplex-specific nuclease-assisted signal amplification, ACS Appl. Mater. Interfaces 8 (2016) 33499–33505.
[30] S. Liu, W. Su, Y. Li, L. Zhang, X. Ding, Manufacturing of an electrochemical biosensing platform based on hybrid DNA hydrogel: taking lung cancer-specific miR-21 as an example, Biosens. Bioelectron. 103 (2018) 1–5.
[31] H. Xu, M. Gao, X. Tang, W. Zhang, D. Luo, M. Chen, Micro/nano Technology for next-generation diagnostics, Small Methods. DOI: 10.1002/smtd.201900506.
[32] S.H. Um, J.B. Lee, N. Park, S.Y. Kwon, C.C. Umbach, D. Luo, Enzyme-catalysed assembly of DNA hydrogel, Nat. Mater. 5 (2006) 797–801.
[33] N.C. Seeman, Nucleic acid junctions and lattices, J. Theor. Biol. 99 (1982) 237–247.
[34] F. Li, J. Tang, J. Geng, D. Luo, D. Yang, Polymeric DNA hydrogel: design, synthesis and applications, Prog. Polym. Sci. 98 (2019) 101163.
[35] B. Xiang, K. He, R. Zhu, Z. Liu, S. Zeng, Y. Huang, Z. Nie, S. Yao, Self-assembled DNA hydrogel based on enzymatically polymerized DNA for protein encapsulation and enzyme/DNAzyme hybrid cascade reaction, ACS Appl. Mater. Interfaces 8 (2016) 22801–22807.
[36] N. Park, S.H. Um, H. Funabashi, J. Xu, D. Luo, A cell-free protein-producing gel, Nat. Mater. 8 (2009) 432–437.
[37] J. Hur, K. Im, S. Hwang, B. Choi, S. Kim, S. Hwang, N. Park, K. Kim, DNA hydrogel-based supercapacitors operating in physiological fluids, Sci. Rep. 3 (2013) 1282.
[38] S. Wang, S. Lu, J. Zhao, J. Ye, J. Huang, X. Yang, An electric potential modulated cascade of catalyzed hairpin assembly and rolling chain amplification for microRNA detection, Biosens. Bioelectron. 126 (2019) 565–571.
[39] M. Xu, J. Ye, D. Yang, A.A. Abdullah AL-maskri, H. Hu, C. Jung, S. Cai, S. Zeng, Ultrasensitive detection of miRNA via one-step rolling circle-quantitative PCR (RC-qPCR), Anal. Chim. Acta 1077 (2019) 208–215.
[40] L. Zhou, Y. Wang, C. Yang, H. Xu, J. Luo, W. Zhang, X. Tang, S. Yang, W. Fu, K. Chang, M. Chen, A label-free electrochemical biosensor for microRNAs detection based on DNA nanomaterial by coupling with Y-shaped DNA structure and non-linear hybridization chain reaction, Biosens. Bioelectron. 126 (2019) 657–663.
[41] J. Chen, Y. Zhuo, X. Peng, Y. Chai, R. Yuan, W. Liang, A dynamic DNA machine via free walker movement on lipid bilayer for ultrasensitive electrochemiluminescent bioassay, Anal. Chem. 91 (2019) 14125–14132.
[42] L. Tian, J. Qi, X. Ma, X. Wang, C. Yao, W. Song, Y. Wang, A facile DNA strand displacement reaction sensing strategy of electrochemical biosensor based on N-carboxymethyl chitosan/molybdenum carbide nanocomposite for microRNA-21 detection, Biosens. Bioelectron. 122 (2018) 43–50.
[43] J. Liu, Y. Zhang, H. Xie, L. Zhao, L. Zheng, H. Ye, Applications of catalytic hairpin assembly reaction in biosensing, Small 15 (2019), e1902989.
[44] L. Zhao, R. Sun, P. He, X. Zhang, Ultrasensitive detection of exosomes by

target-triggered three-dimensional DNA walking machine and exonuclease III-assisted electrochemical ratiometric biosensing, Anal. Chem. 91 (2019) 14773–14779.
[45] Y. Chen, K. Huang, K. Niu, Recent advances in signal amplification strategy based on oligonucleotide and nanomaterials for microRNA detection-a review, Biosens. Bioelectron. 99 (2018) 612–624.
[46] C. Bica-Pop, R. Cojocneanu-Petric, L. Magdo, L. Raduly, D. Gulei, I. Berindan-Neagoe, Overview upon miR-21 in lung cancer: focus on NSCLC, Cell, Mol. Life Sci. 75 (2018) 3539–3551.
[47] D. Sekar, P. Mani, M. Biruntha, P. Sivagurunathan, M. Karthigeyan, Dissecting the functional role of microRNA 21 in osteosarcoma, Canc. Gene Ther. 26 (2019) 179–182.
[48] A. Larrabeiti-Etxebarria, M. Lopez-Santillan, B. Santos-Zorrozua, E. Lopez-Lopez, A. Garcia-Orad, Systematic review of the potential of MicroRNAs in diffuse large B cell lymphoma, Cancers 11 (2019) 144.